CrystEngComm

COMMUNICATION

View Article Online
View Journal | View Issue

Cite this: *CrystEngComm*, 2017, **19**, 6927

Received 14th September 2017,
Accepted 28th October 2017

DOI: 10.1039/c7ce01649b

rsc.li/crystengcomm

Pre-design and synthesis of a five-fold interpenetrated pcu-type porous coordination polymer and its CO_2/CO separation†

Haifei Cao,[a] Suna Wang,[b] Yang Wang,[a] HongLiang Lyu,[a] Rajamani Krishna,[c] Zhiyong Lu,*[d] Jingui Duan*[a] and Wanqin Jin[a]

From the viewpoint of mathematics and topology, we proposed a rational design and stabilized the first five-fold interpenetrated porous coordination polymer (PCP) with a **pcu** topology and extra-framework volume (60.0%) by employing a linear ligand with the length of ~2 nm. The resulting compound exhibits good CO_2 uptake, enabling highly selective separation of CO_2 from CO_2/CO mixtures.

Interpenetrated PCPs with significant available space have attracted significant interest in porous material synthesis as they usually show fascinating architectures and topologies as well as optimized functions and applications.[1] It is known that the origin of interpenetration in PCP can be ascribed to the existence of free volume in a single network that allows catenation from another or more same networks to form a 2-fold or greater interpenetrated network.[2] Consequently, interpenetration was believed to be a drawback, which harmed the porosity and became worse in PCPs with higher degrees of interpenetration. However, accompanying the rapid development of PCP chemistry, many important advances in the field of interpenetrated PCPs have been achieved.[1f,2b,3] The diversified and controllable structures often endow increased volumetric density uptakes,[4] improved interactions between a host and guest,[1g,3b,5] as well as promoted framework stability.[6] More interestingly, interpenetration often brings flexibility in PCPs; this indicates the existence of a unique dynamic response by guest stimulus that is helpful for highly selective guest capture and separation.[1h,2b,3b] Despite these, the fine tuning or control of the network interpenetration within the accurate blueprint remains a great challenge, especially for integrated domains with huge cages, higher degrees of interpenetration (higher than 4-fold), and high porosity.[7]

To fulfill this goal, several strategies have been investigated such as changing the pH,[8] template,[4a] solvent,[9] reaction temperature,[3d] and concentration of the starting material,[3d] as well as liquid phase epitaxial growth[1f] and sonochemical synthesis with powder level adjustment.[10] Indeed, these methods worked well in tuning the interpenetrated frameworks. For example, Yaghi and co-workers used a synthetic strategy employing secondary building units (SBUs) to achieve a PCP with a large free volume and functionalized open networks. The size of SBUs was too large to fit in the space remaining after two interpenetrating frameworks formed; this led to the large free volume.[7] In addition, they constructed a 4-fold interpenetrated PCP, MOF-1000, with a **pcu** topology by utilizing a longer ligand.[11] Chen and co-workers successfully obtained a non-interpenetrated microporous PCP (UTSA-68) over a two-fold form (ZJU-30) by changing the pH modifier from concentrated HCl to HBF_4.[12] Zhou and co-workers utilized the method of addition of oxalic acid to avoid interpenetration in synthesis of PCN-6′.[4b] However, from a structural point of view, the deliberate organic linkers and metal nodes played the most important role in the formation of PCPs with high degree of interpenetration.[13]

We are interested in the design, development, and control of functional PCPs for promising gas storage and separation.[4a,14] In one of our previous reports, we controlled the shifting degree of the **pcu** interpenetrated framework by tuning the template and temperature; this resulted in enlarged pore sizes in the range from 5.8 × 4.2 Å^2 to 11.1 × 10.8 Å^2 and enhanced hydrogen uptake.[4a] It is worth noting that

[a] *State Key Laboratory of Materials-Oriented Chemical Engineering, College of Chemical Engineering, Jiangsu National Synergetic Innovation Centre for Advanced Materials, Nanjing Tech University, Nanjing, 210009, China. E-mail: duanjingui@njtech.edu.cn*

[b] *Shandong Provincial Key Laboratory of Chemical Energy Storage and Novel Cell Technology, School of Chemistry and Chemical Engineering, Liaocheng University, Liaocheng, 252059, China*

[c] *Van't Hoff Institute for Molecular Sciences, University of Amsterdam, Science Park 904, 1098 XH Amsterdam, The Netherlands*

[d] *College of Mechanics and Materials, Hohai University, Nanjing 210098, China. E-mail: johnlook1987@gmail.com*

† Electronic supplementary information (ESI) available: Ligand synthesis, TG, PXRD, adsorption heats and information for IAST and breakthrough simulation. CCDC of **NTU-26** is 1574418. For ESI and crystallographic data in CIF or other electronic format see DOI: 10.1039/c7ce01649b

the 2-fold interpenetrated mother PCP has been prepared by extending the linker from a length of l (from H_2BDC in MOF-5)[15] to $\sqrt{2}l$ (from 4,4′-(carbonylimino)dibenzoic acid (H_2L^1) in NJU-Bai1), in combination with the 6-connected $Zn_4O(COO)_6$ clusters (Fig. 1a–e). Although l has a fixed value in H_2BDC, the defined length of $\sqrt{2}l$ should be considered as a rational range for the PCP design. This is why another series of 2-fold interpenetrated **pcu** PCPs, featuring variable cavities, was also prepared from dicarboxylate ligands with varied lengths.[9a,16] Theoretically, according to this rule, if the length of the linear ligand reaches $\sqrt{5}l$, a five-fold interpenetrated framework can be constructed (Fig. 1a, f, and g).

Inspired by this view, a multifunctional linear ligand (4,4′-[1,4-phenylenebis(carbonylimino)]-bis[benzoic acid]: H_2L^2) with a length of 2 nm (2.8 times of H_2BDC) was deliberately designed to not only include a long aromatic and semi-rigid dicarboxylate scaffold, but also offer promising characteristics such that it possesses two amide groups around the middle benzene. A solvothermal reaction of H_2L^2 and zinc(II) nitrate affords a new five-fold interpenetrated PCP, (**NTU-26**), with an extra-framework volume of up to 60.0%, despite its five-fold interpenetration. Remarkably, it is the first example of five-fold interpenetrated PCP with a **pcu** topology. In addition, gas adsorption and breakthrough simulation showed that **NTU-26** exhibited high potential for adsorption-based CO_2/CO separation at ambient temperature.

The solvothermal reaction of zinc(II) nitrate with H_2L^2 in DEF afforded block-shaped crystals at 80 °C in 24 hours. Single-crystal X-ray diffraction revealed that $[Zn_4O(L)_3{\cdot}2H_2O]$·solvent (**NTU-26**) crystallizes in the space group of $P\bar{1}$ with a = 11.2432(15) Å, b = 21.829(3) Å, and c = 25.837(4) Å (Table S1†). The asymmetric unit includes four crystallographically independent Zn(II) ions, three carboxylate ligands, one μ^4-O^{2-} ion, and two coordinated water molecules (Fig. S1†). Zn1, Zn2, and Zn4 show similar tetrahedral coordination geometry, and each of them is surrounded by three oxygen atoms from three different carboxylate groups and the μ^4-O^{2-} ion, situated at the center of four Zn ions. Moreover, six coordinated Zn3 formed an octahedron as an additional coordination occurred from two water molecules (Fig. S2†). Despite these changes, the $Zn_4O(COO)_6$ cluster herein presents as a six-connected node. Due to the semi-rigidity of H_2L^2, an ellipsoid space was found within its huge cage. Vertically and axially, the size of this object was ~25 Å, whereas the value increased to ~40 Å horizontally (Fig. 2a). The huge pore and involved hydrogen bonding from amide groups, carboxylate groups, and coordinated water molecules direct the formation and positioning of another four frameworks; thus, the five-fold interpenetrated **pcu** network is formed (Fig. 2b). Despite its five-fold interpenetration, **NTU-26** possesses two-dimensional open channels with significant window apertures of 5.2 × 8.0 $Å^2$, 6.3 × 8.0 $Å^2$, and 4.5 × 7.1 $Å^2$ along the a or b axis (Fig. S5 and S6†). Calculated by PLATON/SOLV, the accessible total volume in the desolvated structure of **NTU-26** was estimated to a high value of 60.0%,[17] which corresponded to a low framework density (0.79 g cm^{-3}). For a better understanding of this structure, Fig. 2c–f show the vivid and pictorial impression of framework interpenetration. Generally, the nets from interpenetrated PCP are in the same or reverse direction. However, in this case, three nets weaved in a group, and the other two built up another group with ~30° anticlockwise rotation. Then, two groups of nets interwove with each other to form the final framework. The powder X-ray diffraction (PXRD) pattern of **NTU-26** showed that peak positions of the as-synthesized phase were the same as those for its simulated data, indicating good phase purity (Fig. S8†). Thermogravimetric analysis revealed that **NTU-26** started to decompose at ~380 °C (Fig. S9†).

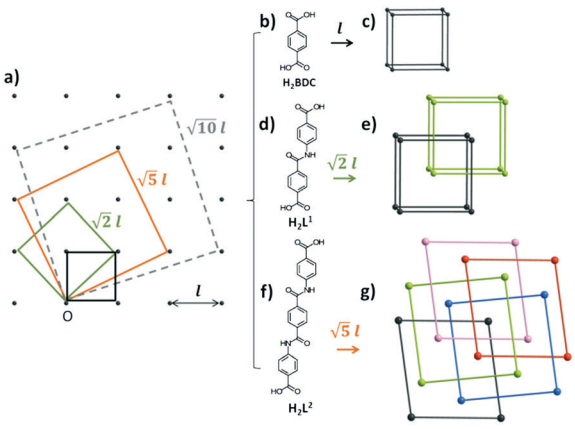

Fig. 1 Evolution of interpenetration phenomenon in PCPs with a **pcu** topology (a): non-interpenetrated framework with the ligand H_2BDC (b and c); 2-fold interpenetrated network with the ligand H_2L^1 (d and e); five-fold interpenetrated network with the ligand H_2L^2 (f and g).

The intriguing structural features and rich amide groups of **NTU-26** prompted us to study its capability for gas storage and separation. To confirm the permanent porosity, **NTU-26** was treated by super-critical CO_2 and then evacuated at 45 °C for 20 hours to obtain the activated framework. Adsorption isotherms of N_2 (77 K), CO_2 (195 K), and CO (195 K) were obtained. As shown in Fig. S10,† the N_2 isotherm revealed a fully reversible type-IV isotherm, but the lower gas uptake before P/P_0 = 0.25 limited the surface area evaluation. As an alternative, the CO_2 isotherm at 195 K was employed to fulfill this task. The calculated BET (Langmuir) surface area of **NTU-26** reached 230 m^2 g^{-1} (380 m^2 g^{-1}), which was lower than the predicted value (1630 m^2 g^{-1}). This may be due to the partial collapse and reduced window aperture of the **NTU-26** framework, supported by such a long linker.

Despite the medium surface area, **NTU-26** displayed quick CO_2 uptake before 20 kPa, and the uptake of CO increased very slowly upon increasing the pressure (Fig. 3a). Importantly, the difference in the uptake amounts at P = 100 kPa (CO_2: 3.3 mmol g^{-1} and CO: 0.5 mmol g^{-1}) showed that **NTU-26** was a good candidate for selective capture of CO_2 from CO_2/CO mixtures. The favorable adsorption of CO_2 to CO by **NTU-26** was further confirmed by adsorption measurements at 273 K (Fig. 3b).

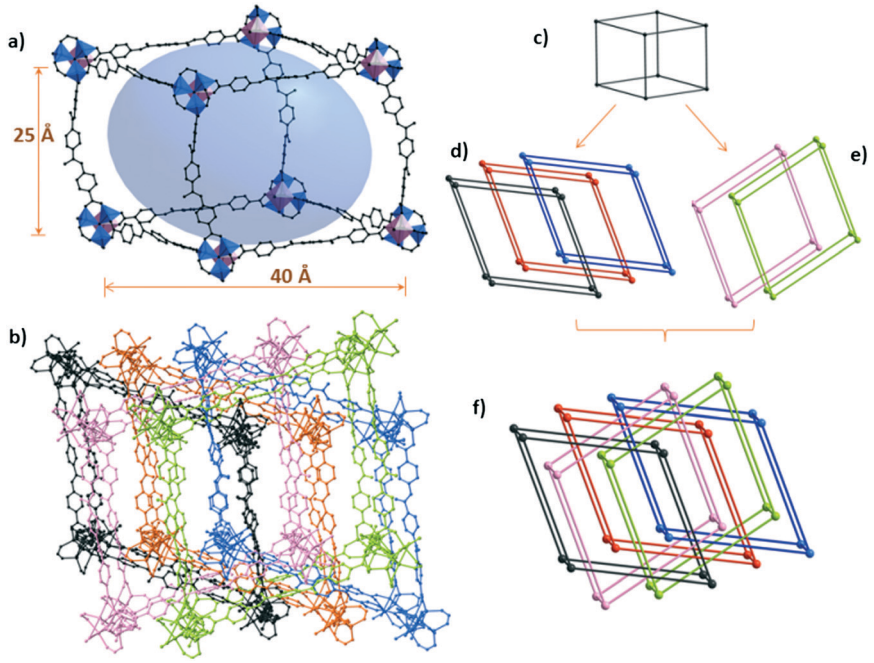

Fig. 2 The structural view of **NTU-26**: (a) single cage with huge ellipsoid space; (b) view of five-fold framework and its potential assessable volume; and (c–f) vivid and pictorial impression of framework interpenetration.

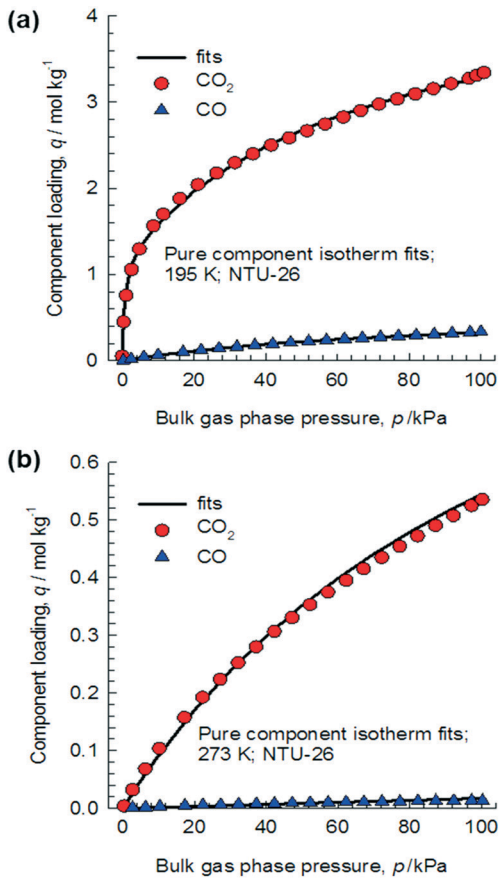

Fig. 3 Comparison of experimental data on component loadings for adsorption of pure components CO and CO_2 in **NTU-26** at (a) 195 K and (b) 273 K with isotherm fits.

The ideal adsorbed solution theory (IAST) of Myers and Prausnitz[18] is an established procedure to describe gas-mixture adsorption in representative zeolites and PCPs, and it has been employed to predict multicomponent adsorption behaviors from the experimental single-component gas isotherms. The component loadings for the adsorption of 80/20 CO/CO_2 mixtures and the predicted adsorption selectivity of **NTU-26** at 273 K are presented in Fig. S11† and 4a, respectively. As expected, the selectivity of CO_2 relative to that of CO was as high as 60 at 1 bar, which was higher than that of ZIF-68 (19.2), La-BTN (27.2)[14d] MCM-41 (37.0),[19] BPL carbon (7.5),[20] and some zeolites (10.2–50.0).[21] To further understand the separation performance, transient breakthrough simulation, using the procedure established in previous works,[22] was also performed in a fixed bed adsorber to investigate its CO_2/CO separation potential, as shown in Fig. 4b. Transient breakthrough simulations reveal that CO breaks through near the start, and purified CO can be recovered during the early stages of the transient breakthrough. To understand this good separation ability, the adsorption enthalpies of CO_2 and CO were calculated. Fig. S12† presents data on the loading dependence of Q_{st} for CO_2 and CO in **NTU-26**. We noted that the Q_{st} of CO_2 (30 kJ mol^{-1}) was significantly higher than that of CO (21 kJ mol^{-1}) at zero coverage.

In summary, we have designed and prepared the first five-fold interpenetrated **pcu**-type PCP from the viewpoint of mathematics and topology. Remarkably, it has a huge cage and extra-framework volume of up to 60.0% despite its five-fold interpenetration. The intriguing structural features and rich amide groups endow **NTU-26** with high potential for selective CO_2 capture from CO_2/CO mixtures at ambient

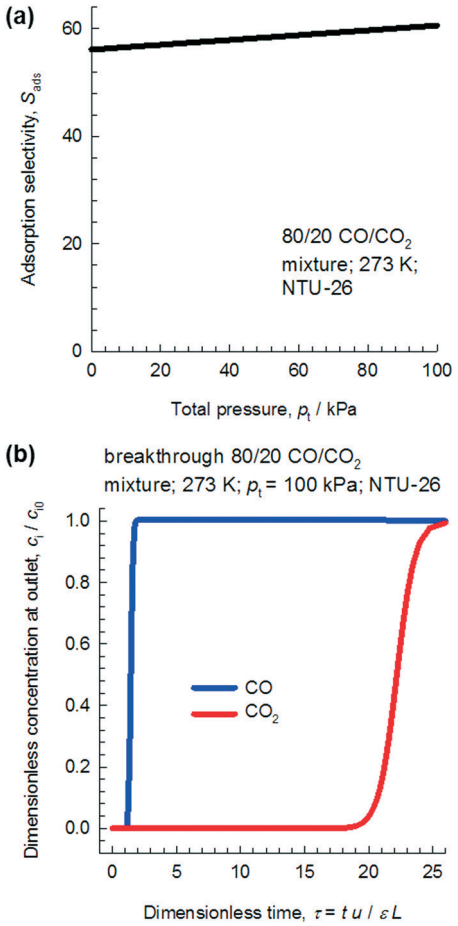

Fig. 4 (a) IAST calculations of CO_2/CO adsorption selectivity for **NTU-26** at 273 K; (b) transient breakthrough simulations for separation of 80/20 CO/CO_2 mixture in a fixed bed packed with **NTU-26** at 273 K. The total inlet pressure was 100 kPa.

temperature. Thus, this study provided not only an unprecedented porous structure with 5-fold interpenetration, but also clear guidance for facilitating research on PCPs with higher degree interpenetration, such as 10-fold.

The authors gratefully acknowledge the financial support received from the National Science Foundation of China (21671102, 21601047 and 21571092), Innovative Research Team Program by the Ministry of Education of China (IRT17R54), National Science Foundation of Jiangsu Province (BK20161538 and BK20150798), Six talent peaks project in Jiangsu Province (JY-030), and State Key Laboratory of Materials-Oriented Chemical Engineering (ZK201406).

Conflicts of interest

There are no conflicts to declare.

References

1 (*a*) S. Bureekaew, H. Sato, R. Matsuda, Y. Kubota, R. Hirose, J. Kim, K. Kato, M. Takata and S. Kitagawa, *Angew. Chem., Int. Ed.*, 2010, **49**, 7660–7664; (*b*) M. H. Zeng, W. X. Zhang, X. Z. Sun and X. M. Chen, *Angew. Chem., Int. Ed.*, 2005, **44**, 3079–3082; (*c*) F. Luo, J. M. Zheng and S. R. Batten, *Chem. Commun.*, 2007, 3744–3746; (*d*) S. Y. Zhang, Z. J. Zhang and M. J. Zaworotko, *Chem. Commun.*, 2013, **49**, 9700–9703; (*e*) H. L. Jiang, T. A. Makal and H. C. Zhou, *Coord. Chem. Rev.*, 2013, **257**, 2232–2249; (*f*) O. Shekhah, H. Wang, M. Paradinas, C. Ocal, B. Schupbach, A. Terfort, D. Zacher, R. A. Fischer and C. Woll, *Nat. Mater.*, 2009, **8**, 481–484; (*g*) R. Babarao, C. J. Coghlan, D. Rankine, W. M. Bloch, G. K. Gransbury, H. Sato, S. Kitagawa, C. J. Sumby, M. R. Hill and C. J. Doonan, *Chem. Commun.*, 2014, **50**, 3238–3241; (*h*) T. K. Maji, R. Matsuda and S. Kitagawa, *Nat. Mater.*, 2007, **6**, 142–148.

2 (*a*) O. M. Yaghi, *Nat. Mater.*, 2007, **6**, 92–93; (*b*) S. H. Yang, X. Lin, W. Lewis, M. Suyetin, E. Bichoutskaia, J. E. Parker, C. C. Tang, D. R. Allan, P. J. Rizkallah, P. Hubberstey, N. R. Champness, K. M. Thomas, A. J. Blake and M. Schroder, *Nat. Mater.*, 2012, **11**, 710–716.

3 (*a*) Y. Yan, M. Juricek, F. X. Coudert, N. A. Vermeulen, S. Grunder, A. Dailly, W. Lewis, A. J. Blake, J. F. Stoddart and M. Schroder, *J. Am. Chem. Soc.*, 2016, **138**, 3371–3381; (*b*) C. Wang, L. J. Li, J. G. Bell, X. X. Lv, S. F. Tang, X. B. Zhao and K. M. Thomas, *Chem. Mater.*, 2015, **27**, 1502–1516; (*c*) P. Li, Y. B. He, H. D. Arman, R. Krishna, H. L. Wang, L. H. Weng and B. L. Chen, *Chem. Commun.*, 2014, **50**, 13081–13084; (*d*) J. J. Zhang, L. Wojtas, R. W. Larsen, M. Eddaoudi and M. J. Zaworotko, *J. Am. Chem. Soc.*, 2009, **131**, 17040–17041; (*e*) J. G. Duan, Q. Q. Li and Z. Y. Lu, *CrystEngComm*, 2015, **17**, 2087–2090.

4 (*a*) J. Duan, J. Bai, B. Zheng, Y. Li and W. Ren, *Chem. Commun.*, 2011, **47**, 2556–2558; (*b*) S. Q. Ma, D. F. Sun, M. Ambrogio, J. A. Fillinger, S. Parkin and H. C. Zhou, *J. Am. Chem. Soc.*, 2007, **129**, 1858–1859.

5 T. Pham, K. A. Forrest, B. Tudor, S. K. Elsaidi, M. H. Mohamed, K. McLaughlin, C. R. Cioce, M. J. Zaworotko and B. Space, *Langmuir*, 2014, **30**, 6454–6462.

6 (*a*) H. Jasuja and K. S. Walton, *Dalton Trans.*, 2013, **42**, 15421–15426; (*b*) J. G. Duan, W. Q. Jin and S. Kitagawa, *Coord. Chem. Rev.*, 2017, **332**, 48–74.

7 T. M. Reineke, M. Eddaoudi, D. Moler, M. O'Keeffe and O. M. Yaghi, *J. Am. Chem. Soc.*, 2000, **122**, 4843–4844.

8 K. P. Rao, M. Higuchi, J. G. Duan and S. Kitagawa, *Cryst. Growth Des.*, 2013, **13**, 981–985.

9 (*a*) J. H. Lee, T. K. Kim, M. P. Suh and H. R. Moon, *CrystEngComm*, 2015, **17**, 8807–8811; (*b*) M. Guo and Z. M. Sun, *J. Mater. Chem.*, 2012, **22**, 15939–15946.

10 J. Kim, S. T. Yang, S. B. Choi, J. Sim, J. Kim and W. S. Ahn, *J. Mater. Chem.*, 2011, **21**, 3070–3076.

11 Q. W. Li, W. Y. Zhang, O. S. Miljanic, C. H. Sue, Y. L. Zhao, L. H. Liu, C. B. Knobler, J. F. Stoddart and O. M. Yaghi, *Science*, 2009, **325**, 855–859.

12 G. G. Chang, B. Li, H. L. Wang, T. L. Hu, Z. B. Bao and B. L. Chen, *Chem. Commun.*, 2016, **52**, 3494–3496.

13 (*a*) D. D. Zhou, Z. J. Liu, C. T. He, P. Q. Liao, H. L. Zhou, Z. S. Zhong, R. B. Lin, W. X. Zhang, J. P. Zhang and X. M. Chen, *Chem. Commun.*, 2015, **51**, 12665–12668; (*b*) Y. N.

Gong, D. C. Zhong and T. B. Lu, *CrystEngComm*, 2016, **18**, 2596–2606.

14 (*a*) Z. Lu, J. Zhang, J. Duan, L. Du and C. Hang, *J. Mater. Chem. A*, 2017, **5**, 17287–17292; (*b*) J. Duan, M. Higuchi, J. Zheng, S. I. Noro, I. Y. Chang, K. Hyeon-Deuk, S. Mathew, S. Kusaka, E. Sivaniah, R. Matsuda, S. Sakaki and S. Kitagawa, *J. Am. Chem. Soc.*, 2017, **139**, 11576–11583; (*c*) M. L. Foo, R. Matsuda, Y. Hijikata, R. Krishna, H. Sato, S. Horike, A. Hori, J. Duan, Y. Sato, Y. Kubota, M. Takata and S. Kitagawa, *J. Am. Chem. Soc.*, 2016, **138**, 3022–3030; (*d*) J. Duan, M. Higuchi, R. Krishna, T. Kiyonaga, Y. Tsutsumi, Y. Sato, Y. Kubota, M. Takata and S. Kitagawa, *Chem. Sci.*, 2014, **5**, 660–666; (*e*) J. G. Duan, M. Higuchi, S. Horike, M. L. Foo, K. P. Rao, Y. Inubushi, T. Fukushima and S. Kitagawa, *Adv. Funct. Mater.*, 2013, **23**, 3525–3530.

15 H. Li, M. Eddaoudi, M. O'Keeffe and O. M. Yaghi, *Nature*, 1999, **402**, 276–279.

16 (*a*) M. Eddaoudi, J. Kim, N. Rosi, D. Vodak, J. Wachter, M. O'Keeffe and O. M. Yaghi, *Science*, 2002, **295**, 469–472; (*b*) P. Y. Guo, D. Y. Ma and H. F. Guo, *Acta Crystallogr., Sect. C: Struct. Chem.*, 2017, **73**, 470–475.

17 A. L. Spek, *J. Appl. Crystallogr.*, 2003, **36**, 7–13.

18 A. L. Myers and J. M. Prausnitz, *AIChE J.*, 1965, **11**, 121–127.

19 F. Nkinahamira, T. Z. Su, Y. Q. Xie, G. F. Ma, H. T. Wang and J. Li, *Chem. Eng. J.*, 2017, **326**, 831–838.

20 R. Banerjee, A. Phan, B. Wang, C. Knobler, H. Furukawa, M. O'Keeffe and O. M. Yaghi, *Science*, 2008, **319**, 939–943.

21 I. Matito-Martos, A. Martin-Calvo, J. J. Gutierrez-Sevillano, M. Haranczyk, M. Doblare, J. B. Parra, C. O. Ania and S. Calero, *Phys. Chem. Chem. Phys.*, 2014, **16**, 19884–19893.

22 (*a*) R. Krishna, *Microporous Mesoporous Mater.*, 2014, **185**, 30–50; (*b*) R. Krishna, *RSC Adv.*, 2015, **5**, 52269–52295; (*c*) R. Krishna, *RSC Adv.*, 2017, **7**, 35724–35737.

Supporting Information

Pre-design and synthesis of a five-fold interpenetrated pcu-type porous coordination polymer and its CO_2/CO separation

Haifei Cao[a], Suna Wang[b], Yang Wang[a], HongLiang Lyu[a], Rajamani Krishna[c], Zhiyong Lu[d,*] Jingui Duan[a,*] and Wanqin Jin[a]

[a] State Key Laboratory of Materials-Oriented Chemical Engineering, College of Chemical Engineering, Jiangsu National Synergetic Innovation Centre for Advanced Materials, Nanjing Tech University, Nanjing, 210009, China. E-mail: duanjingui@njtech.edu.cn

[b] Shandong Provincial Key Laboratory of Chemical Energy Storage and Novel Cell Technology, School of Chemistry and Chemical Engineering, Liaocheng University, Liaocheng, 252059, China.

[c] Van 't Hoff Institute for Molecular Sciences, University of Amsterdam, Science Park 904, 1098 XH Amsterdam, The Netherlands

[d] College of Mechanics and Materials, Hohai University, Nanjing 210098, China. E-mail: johnlook1987@gmail.com

1. General Procedures and Materials

All the reagents and solvents were commercially available and used as received. The elemental analysis was carried out with a Perkin-Elmer 240C elemental analyzer. Thermal analyses were performed on a Universal V3.9A TA Instruments with a heating rate of 10°C/min under flowing nitrogen. The powder X-ray diffraction patterns (PXRD) measurements were carried on a Bruker axs D8 Advance 40kV, 40mA for CuK_{α} (θ= 1.5418 Å) with a scan rate of 0.2 s/deg at room temperature. Simulated powder patterns from single-crystal X-ray diffraction data were generated using Mercury 1.4.2 software. Raman was collected using a Horiba Jobin-Yvon HR800 Raman Spectrometer.

2. Synthesis of the organic building block

4,4'-[1,4-Phenylenebis(carbonylimino)]bis[benzoic acid] (**H_2L^2**) was synthesized according to our previous work[1]. ^{1}H NMR (DMSO) of H_2L: δ/ppm 10.58 (s, 2H), 8.05 (s, 4H), 7.92 (m, 8H). ^{13}C NMR (DMSO) of **H_2L^2**: δ/ppm 170.85, 165.23, 144.08, 137.79, 130.85, 127.82, 126.65, 119.96.

3. Synthesis of NTU-26

$Zn(NO_3)_2 \cdot 3H_2O$ (20 mg) and H_2L (10 mg) were mixed with 4 ml of DEF in a glass container and tightly capped with a Teflon vial and heated at 80 °C for two days. After cooling to room temperature, colourless and block shaped crystals were obtained. Yield: ~80% (based on ligand).

4. Single X-ray study

Single-crystal X-ray diffraction data were measured on a Bruker Smart Apex CCD diffractometer at 293 K using graphite monochromated Mo/Kα radiation (λ = 0.71073 Å). Data reduction was made with the Bruker Saint program. The crystal of NJU-Bai3 was mounted in a flame sealed capillary containing a small amount of mother liquor to prevent desolvation during data collection, and data were collected at 298K. The structures were solved by direct methods and refined with full-matrix least squares technique using the SHELXTL package[2]. Non-hydrogen atoms were refined with anisotropic displacement parameters during the final cycles. Organic hydrogen atoms were placed in calculated positions with isotropic displacement parameters set to 1.2×Ueq of the attached atom. The hydrogen atoms of the ligand and water molecules could not be located, but are included in the formula. The unit cell includes a large region of disordered solvent molecules, which could not be modelled as discrete atomic sites. We employed PLATON/SQUEEZE[3] to calculate the diffraction contribution of the solvent molecules and, thereby, to produce a set of solvent-free diffraction intensities; the structure was then refined again using the data generated. The crystal data are reported in Table S1.

Table S1. Crystal data and structure refinement for **NTU-26** at 293 K

	NTU-26
Empirical formula	$C_{66}H_{46}Zn_4O_{21}$
Formula weight	1520.65
Crystal system	triclinic
Space group	*P-1*
Unit cell dimensions	*a* = 11.2432(15) Å *b* = 21.829(3) Å *c* = 25.837(4) Å *α* = 98.929(2)° *β* = 92.438(2)° *γ* = 94.814(2)°
Volume	6232.2(15) $Å^3$
Z	2
Density (calculated)	0.810 g/cm^3
Mu(MoKa)	0.803 mm^{-1}
$F_{(000)}$	1544
Theta min-max	1.9, 25.0
Index ranges	-12<=h<=13 -26<=k<=25 -17<=l<=30
Tot., Uniq. Data, R(int)	31713, 21754, 0.112
Observed data [I > 2σ (I)]	9187
*N*ref, *N*par	21754, 875
R_1, wR_2, S	0.0845, 0.2302, 1.03
Max Shift	0

$R = \Sigma||F_o|-|F_c||/\Sigma|F_o|$, $wR = \{\Sigma[w(|F_o|^2 - |F_c|^2)^2]/\Sigma[w(|F_o|^4)]\}^{1/2}$ and $w = 1/[\sigma^2(F_o^2) + (0.1452P)^2]$ where $P = (F_o^2+2F_c^2)/3$

Table S2. Hydrogen bond in NTU-26.

D—H..A	$d_{H..A}$ (Å)	$d_{D—A}$ (Å)	A_{D-H-A} (°)
N5-- H5A..O3	2.5600	3.271(8)	131.00
N6-- H6A.. O8	2.4000	3.187(8)	138.00
C4-- H4.. O20	2.2600	2.873(15)	123.00
C20-- H20.. O9	2.4600	2.787(13)	100.00
C21-- H21.. O22	2.2500	2.809(18)	118.00
C26-- H26.. O17	2.3000	2.868(12)	118.00
C35-- H35.. O18	2.4200	2.753(16)	101.00
C39-- H39.. O18	2.1700	2.774(15)	122.00
C48-- H48.. O19	2.2400	2.828(11)	120.00
C51-- H51.. O4	2.4500	2.762(9)	100.00
C61-- H61.. O16	2.3500	2.851(11)	114.00
C62-- H62.. O15	2.4100	2.724(10)	100.00
C65-- H65B .. O3	2.4500	3.359(9)	167.00
C66-- H66B .. O16	2.4200	2.745(10)	101.00

5. Sample activation

Before the supercritical CO_2 treatment, as-synthesized samples were soaked in absolute DMF, replacing the soaking solution every 24 h for 3 days. After exchanging, the DMF-containing samples were placed inside the supercritical CO_2 dryer and the DMF was exchanged with CO_2 over a period of 4 h. During this time the liquid CO_2 was vented under positive pressure for five minutes every two hours. The rate of venting of CO_2 was always kept below the rate of filling so as to maintain a full drying chamber. Following venting, the chamber was sealed and the temperature was raised to 40 ºC, at which time the chamber was slowly vented over the course of 15 h. The collected sample was transferred into the sample tube and activated under a dynamic high vacuum at room temperature for overnight to obtain the desolvated sample.

6. Adsorption experiments

In the gas sorption measurement, Ultra-high-purity grade, N_2, CO and CO_2 gases (99.995% purity) were used throughout the adsorption experiments. All of the measured sorption isotherms have been repeated several times to confirm the reproducibility within experimental error. Low-pressure N_2, CO_2 and CH_4 adsorption measurements (up to 1 bar) were performed on BEL mini analyzer. To provide high accuracy and precision in determining P/P_0, the saturation pressure P_0 was measured throughout the N_2 analyses by means of a dedicated saturation pressure transducer, which allowed us to monitor the vapor pressure for each data point. The pore size distribution was obtained from the GCMC method in the BEL mini software package based on the N_2 sorption at 77K.

7. Fitting of pure component isotherms

The isotherm data for CO, and CO_2 in NTU-26 were measured at two different temperatures 195 K, and 273 K. The data were fitted with either the single-site Langmuir or the Dual-site Langmuir model

$$q = q_{A,sat}\frac{b_A p}{1+b_A p} + q_{B,sat}\frac{b_B p}{1+b_B p} \qquad (1)$$

The Langmuir parameters for each site is temperature-dependent

$$b_A = b_{A0}\exp\left(\frac{E_A}{RT}\right); \quad b_b = b_{B0}\exp\left(\frac{E_B}{RT}\right);$$

The single-site, or dual-site Langmuir parameters are provided in Table S3.

8. Isosteric heat of adsorption

The binding energies of CO, and CO_2 in NTU-26 are reflected in the isosteric heat of adsorption, Q_{st}, defined as

$$Q_{st} = RT^2 \left(\frac{\partial \ln p}{\partial T} \right)_q \qquad (2)$$

These values were determined using the pure component isotherm fits using Clausius-Clapeyron equation.

9. IAST calculations of adsorption selectivity

In order to determine the CO_2/CO separation potential of NTU-26, IAST calculations of 80/20 mixture adsorption were performed. Figure S8 shows IAST calculations of the component loadings for adsorption of 80/20 CO/CO_2 mixtures in NTU-26 at 273 K. The adsorption selectivities are determined from

$$S_{ads} = \frac{q_1 / q_2}{p_1 / p_2} \qquad (3)$$

In equation (3), q_1, and q_2 are the molar loadings in the adsorbed phase in equilibrium with the bulk gas phase with partial pressures p_1, and p_2.

10. Transient breakthrough of mixtures in fixed bed adsorbers

The performance of industrial fixed bed adsorbers is dictated by a combination of adsorption selectivity and uptake capacity. For a proper evaluation of NTU-26, we perform transient breakthrough simulations using the simulation methodology described in the literature.[4] For the breakthrough simulations, the following parameter values were used: length of packed bed, L = 0.3 m; voidage of packed bed, ε = 0.4; superficial gas velocity at inlet, u = 0.04 m/s. The transient breakthrough simulation results are presented in terms of a *dimensionless* time, τ, defined by dividing the actual time, t, by the characteristic time, $\frac{L\varepsilon}{u}$.

Table S3. *T*-dependent dual-site Langmuir parameters for CO, and CO_2 in **NTU-26**.

	Site A			Site B		
	$q_{A,sat}$ mol/kg	b_{A0} Pa^{-1}	E_A kJ mol^{-1}	$q_{B,sat}$ mol/kg	b_{B0} Pa^{-1}	E_B kJ mol^{-1}
CO	0.63	3.07×10^{-11}	20.7			
CO_2	1.2	1.5×10^{-11}	30	3.5	4.49×10^{-17}	43

11. Structure of NTU-26

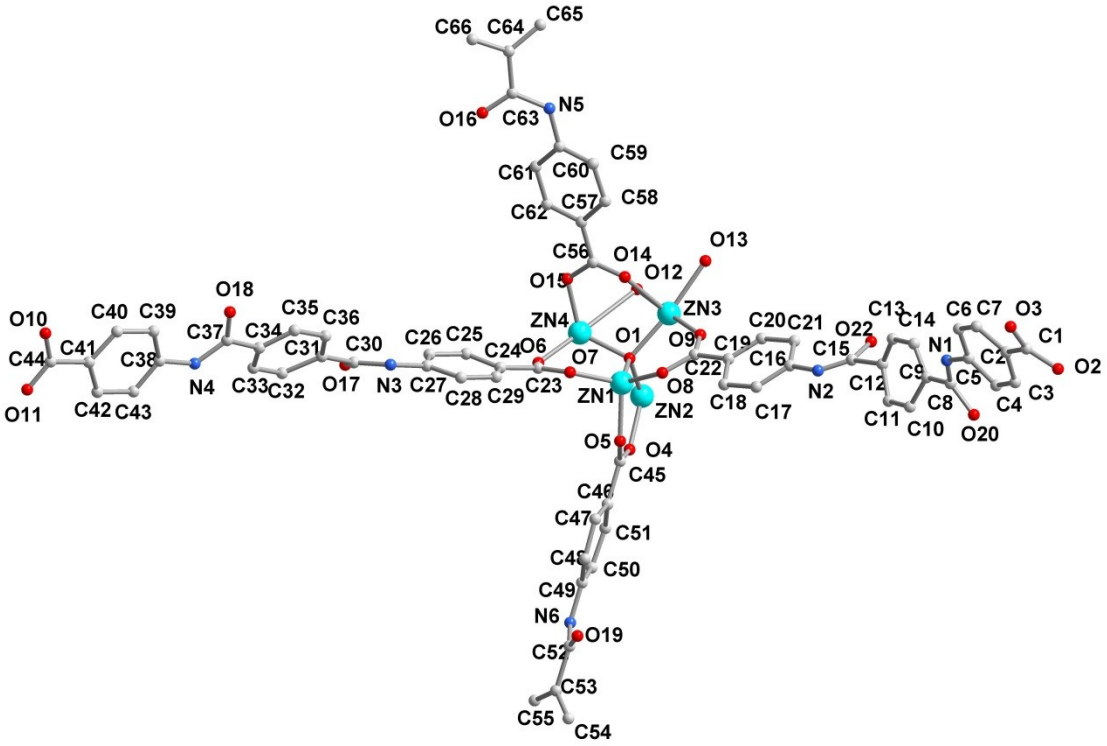

Fig. S1 View of the asymmetric unit of **NTU-26**.

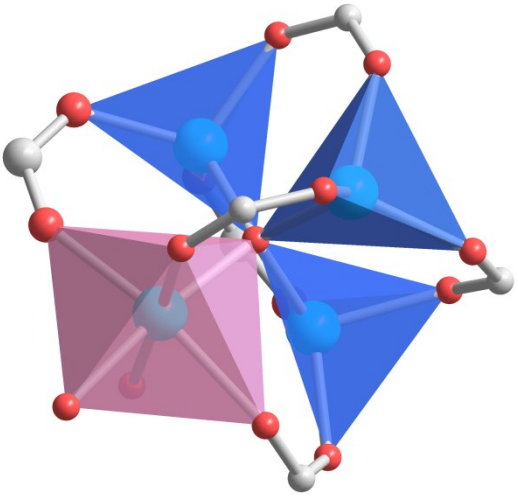

Fig. S2 View of coordination geometry of four zinc atoms in the cluster of **NTU-26:** three tetrahedrons (blue) and a hexahedron (pink).

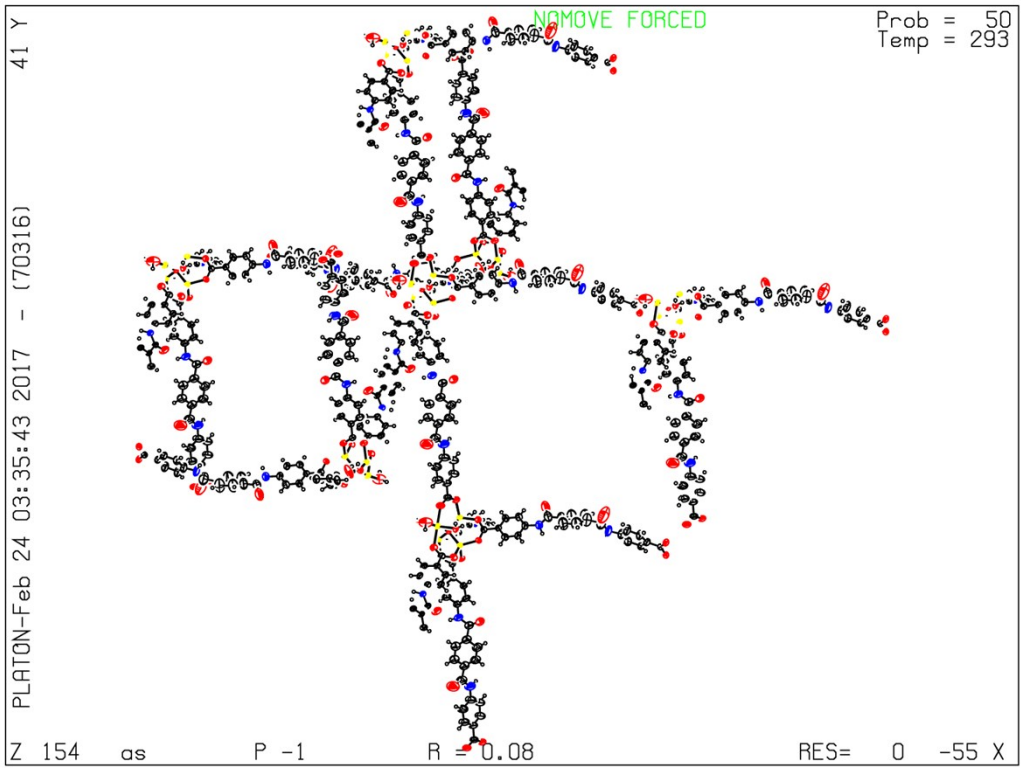

Fig. S3 Thermal ellipsoids of **NTU-26**, drawn at 50% probability.

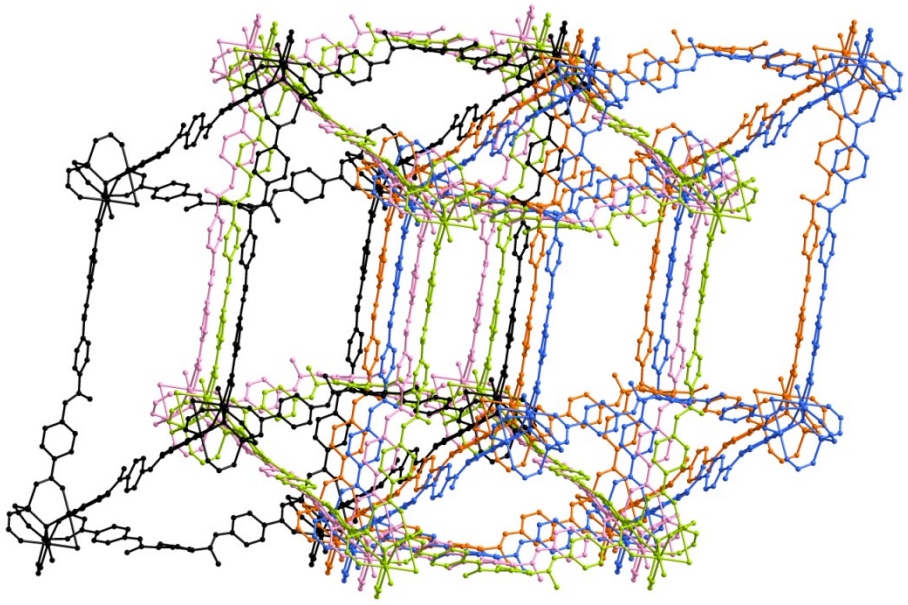

Fig. S4 View of the five-fold interpenetrated **NTU-26**.

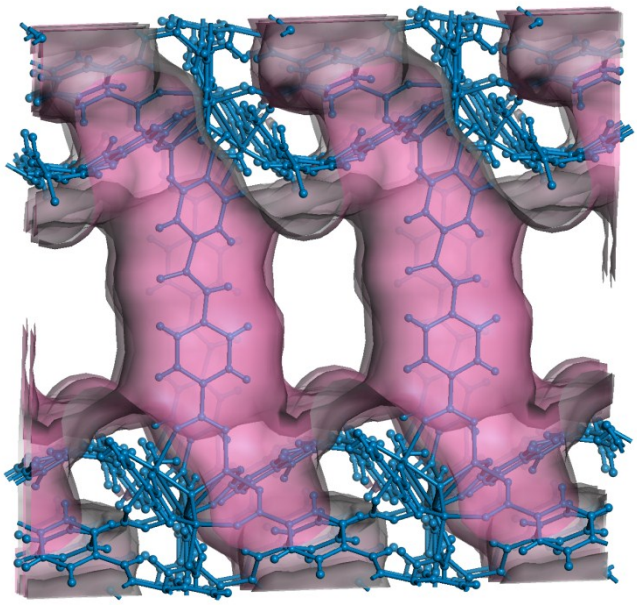

Fig. S5 Packing view of **NTU-26** along b-axis: one channel with size of 4 × 7 Å^2.

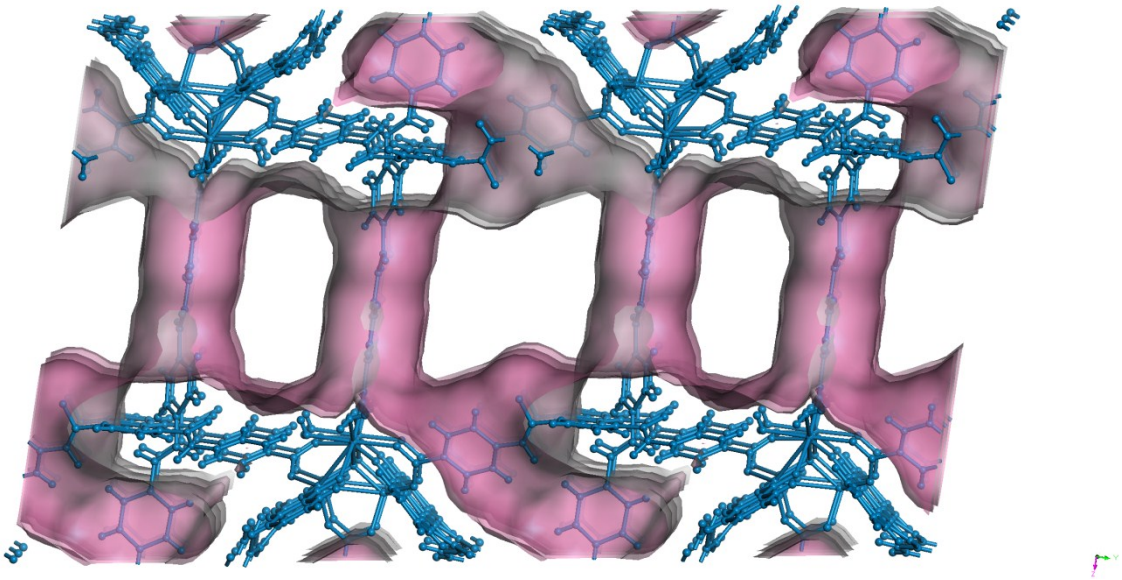

Fig. S6 Packing view of **NTU-26** along a-axis: two kinds of channel with significant window aperture of 5 × 8 Å^2, 6 × 8 Å^2.

12. Characterization of NTU-26

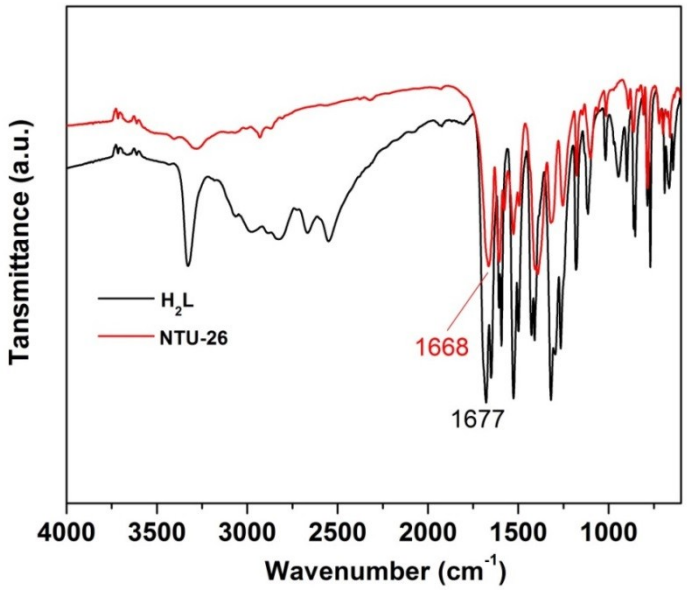

Fig. S7 IR of **H_2L^2** and as-synthesized **NTU-26**: the peak shift from 1677 cm^{-1} to 1668 cm^{-1}, indicating the coordination of carboxylate group.

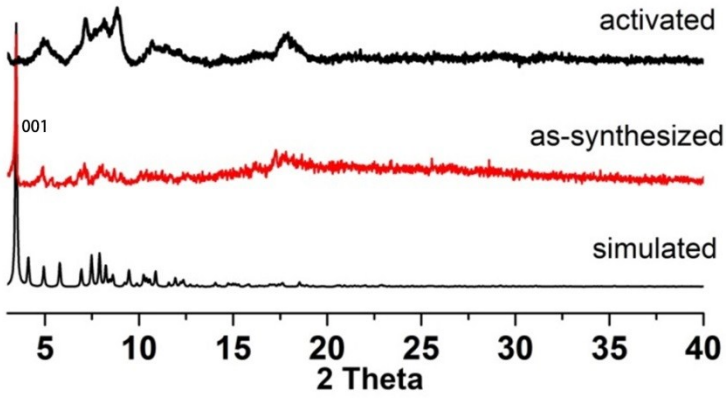

Fig. S8 PXRD of **NTU-26**. For as-synthesized phase, the diffraction peak of 001 plane matches well with simulated data. However, during the measurement, the lost solvent results in decreased crystallinity of NTU-26, as its high extra-framework volume (60.0%). For activated phase, the changed diffraction peaks may be due to the partial collapse of **NTU-26** framework, supported by such long linker.

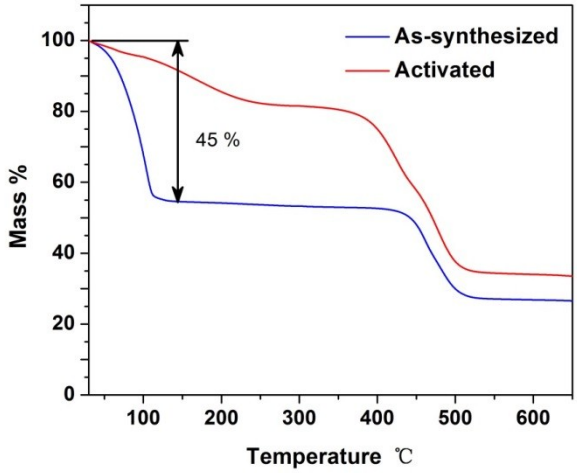

Fig. S9 TG of NTU-26. Before 150 ℃, the TG curve shows that the weight loss is 45% that coincides with loss of DEF and H_2O molecules. Then, the continued weight loss corresponds to the decomposition of the ligands around 420 ℃, and the final solid product at maybe ZnO.

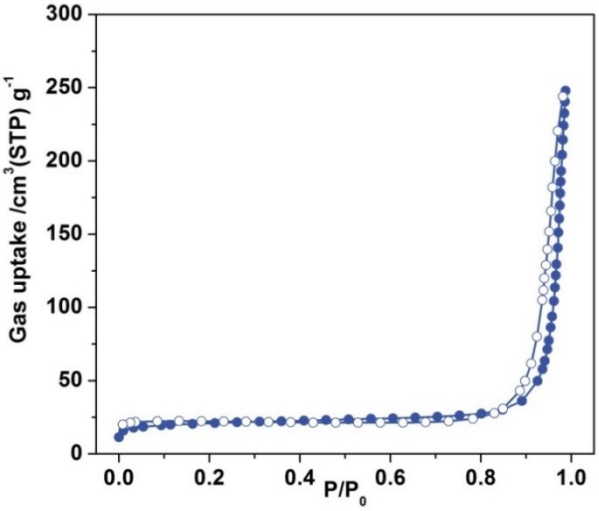

Fig. S10 N_2 adsorption of NTU-26 at 77K.

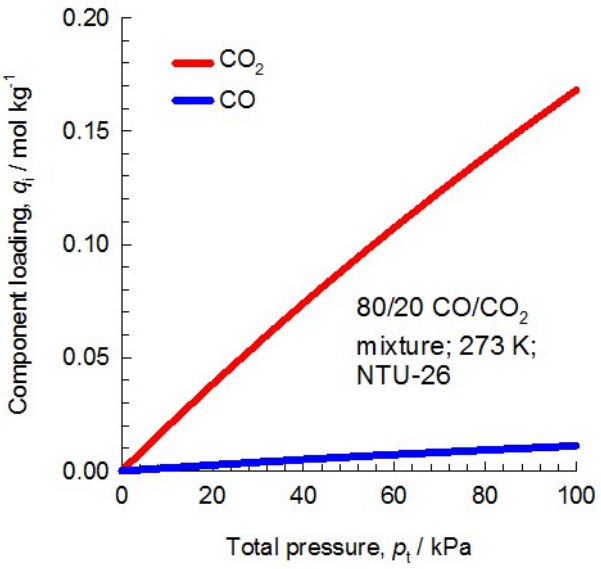

Fig. S11 IAST calculations of the component loadings for adsorption of 80/20 CO/CO_2 mixtures in **NTU-26** at 273 K.

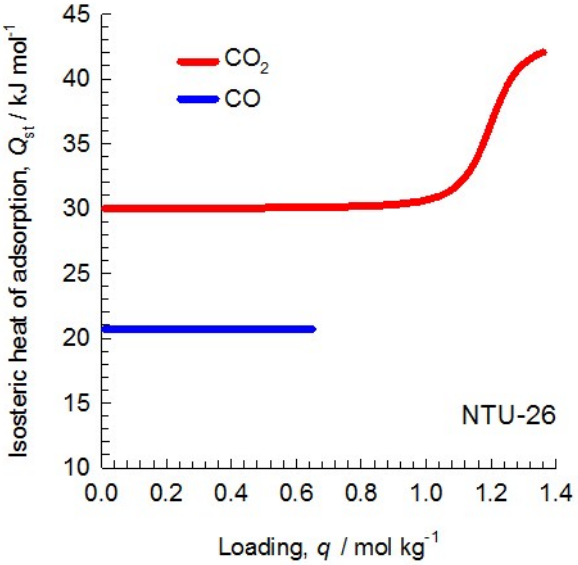

Fig. S12 The isosteric heat of adsorption, Q_{st}, for CO and CO_2 in **NTU-26.** The determination of the Q_{st} is based on the Clausius-Clapeyron equation.

Table S4. Comparison of CO_2/CO selectivity by different porous materials.

PCPs	Predicted CO_2/CO selectivity	Temperature	Refs
MCM-41	37.0	293	[5]
BPL carbon	7.5	273	[6]
I-AC	4.5	298	[7]
ZIF-68	19.2	273	[6]
ZIF-69	20.9	273	[6]
ZIF70	37.8	273	[6]
LaBTN	27.2	273	[8]
some zeolites	10.2-50.0	273	[9]
NTU-26	58.5	273	This work

13. Notation

b Langmuir constant, Pa^{-1}

p_i partial pressure of species *i* in mixture, Pa

p_t total system pressure, Pa

q_i component molar loading of species *i*, mol kg^{-1}

q_t total molar loading in mixture, mol kg^{-1}

q_{sat} saturation loading, mol kg^{-1}

L length of packed bed adsorber, m

R gas constant, 8.314 J mol^{-1} K^{-1}

t time, s

T absolute temperature, K

u superficial gas velocity in packed bed, m s^{-1}

14. Greek letters

ε voidage of packed bed, dimensionless

τ time, dimensionless

15. Subscripts

i referring to component *i*

t referring to total mixture

16. Refs

1. (a)J. Duan, Z. Yang, J. Bai, B. Zheng, Y. Li and S. Li, *Chem. Commun.*, 2012, **48**, 3058-3060; (b)J. Duan, J. Bai, B. Zheng, Y. Li and W. Ren, *Chem. Commun.*, 2011, **47**, 2556-2558.
2. G. M. Sheldrick, *Acta Crystallogr. Sec. A*, 2008, **64**, 112-122.
3. (a)P. Vandersluis and A. L. Spek, *Acta Crystallogr. Sec. A*, 1990, **46**, 194-201; (b)A. L. Spek, *J. Appl. Crystallogr.*, 2003, **36**, 7-13.
4. (a)R. Krishna, *Microporous Mesoporous Mater.*, 2014, **185**, 30-50; (b)R. Krishna, *RSC Advances*, 2015, **5**, 52269-52295; (c)R. Krishna, *RSC Advances*, 2017, **7**, 35724-35737.
5. F. Nkinahamira, T. Z. Su, Y. Q. Xie, G. F. Ma, H. T. Wang and J. Li, *Chem. Eng. J.*, 2017, **326**, 831-838.
6. R. Banerjee, A. Phan, B. Wang, C. Knobler, H. Furukawa, M. O'Keeffe and O. M. Yaghi, *Science*, 2008, **319**, 939-943.
7. B. Mu and K. S. Walton, *J. Chem. Eng. Data*, 2011, **56**, 390-397.
8. J. Duan, M. Higuchi, R. Krishna, T. Kiyonaga, Y. Tsutsumi, Y. Sato, Y. Kubota, M. Takata and S. Kitagawa, *Chem. Sci.*, 2014, **5**, 660-666.
9. I. Matito-Martos, A. Martin-Calvo, J. J. Gutierrez-Sevillano, M. Haranczyk, M. Doblare, J. B. Parra, C. O. Ania and S. Calero, *Phys. Chem. Chem. Phys.*, 2014, **16**, 19884-19893.